An experimental investigation on the performance of shared pile anchors in saturated sand and clay

J. Cui
Southeast University, Nanjing, China, jianbincui@seu.edu.cn

Y. Huang, C. Wu, Y. Zhang
Southeast University, Nanjing, China, yinghuang@seu.edu.cn, chuhengwu@ seu.edu.cn, youhuzhang@seu.edu.cn

ABSTRACT: Shared anchoring, an emerging technology proposed in recent years for floating offshore wind farms, reduces the number of anchors by sharing the anchors between adjacent turbines, thereby reduces the costs for site investigation, fabrication and installation of anchors. Due to phase differences among the different mooring lines of a shared anchor, the resultant force direction varies around the mean direction within an angular range. To shed light on the bearing characteristics of shared pile anchor under this loading condition, results of a series of model tests in saturated sand and clay are reported in this paper. The experimental results in both sand and clay reveal that under multi-directional loading, the failure mechanisms resemble those for fixed-direction loading. The horizontal cumulative displacement of the pile anchor aligns with the mean direction of the resultant force, and its magnitude increases progressively with the number of cycles. Multi-directional loading is shown to accelerate the development of permanent displacement of the anchor under cyclic loading. This effect intensifies with the load level.

1 INTRODUCTION

The mooring and anchoring system secures operation of floating offshore wind turbines. It accounts for 20-25% of the total CapEx (GWEC, 2022). Therefore, innovation to reduce the cost for the anchors is highly relevant for reducing the overall cost of floating offshore wind. In recent years, the concept of shared anchoring has garnered increasing attention (Fontana et al., 2019; Herduin, 2019; Lee and Aubeny, 2020; Yan et al., 2024; Barron et al., 2025). By sharing the same anchor between adjacent wind turbines, shared anchoring reduces the number of anchors required for a wind farm (Xu et al., 2024). The concept was first proposed by Huang and Aggidis (2008) for floating wave energy converters and has been extended to floating offshore wind turbines (Chung, 2012; Diaz et al., 2016). For a large floating offshore wind farm with each turbine secured by three mooring lines, adopting the shared anchoring technology can theoretically reduce the total number of required anchors by 2/3 (Fontana, 2019). In 2023, the Hywind Tampen project was commissioned, which is the first project in the world adopting the shared anchor technology. In this project, only 19 anchors were deployed for securing 11 turbines (Frossard et al., 2025).

Unlike single line anchors which are subjected to tension in fixed direction, shared anchors connected to multiple mooring lines experience multi-directional loading. Researchers have conducted in-depth research on the loading characteristics of shared anchors. Under aligned wind, wave and current conditions, Fontana (2019) found that the mean direction of the resultant load on a shared anchor connected to three lines is aligned with the environment. However, an angular range about 30º is observed which is due to phase differences among the different mooring lines connected to the same anchor. Lovera et al. (2025) further found that misaligned wind and wave can lead to net tension on a shared anchor to vary within an angular range.

Pile anchors are widely adopted for mooring various offshore floating structures, which are natural candidate for shared anchors due to isotropic holding capacity. In recent years, a number of studies have been conducted to investigate the responses of pile anchors under multi-directional conditions by means of 1g and Ng model testing (Herduin, 2019; Chalhoub et al., 2025; Huang et al., 2025; Zabatta et al., 2025) and by numerical simulations (Jenck et al., 2021; Dias et al., 2025). Chalhoub et al. (2025) and Zabatta et al. (2025) investigated the response of shared pile anchors in dense sand by model testing in which a fixed load is applied in one direction while cyclic load is applied in the orthogonal direction. This loading condition was found to result in greater cumulative displacements of the pile anchor as compared to single axis cyclic loading. However, the response of shared pile anchors under cyclic loading with the resultant direction varying within an angular range remains unclear.

To fill this knowledge gap, a series of model tests on shared pile anchors in both saturated sand and clay are carried out using custom-developed testing set-ups. This study systematically investigates the failure mechanism and load-displacement behaviours of shared pile anchor under cyclic loading with the resultant direction varying within an angular range. The research findings provide critical insights on the failure mechanisms of shared piles anchors thus paves the foundation for developing practical design methodologies of shared anchors in deep-water floating wind farm applications.

2 TEST METHOD

2.1 Testing set-up

To apply multi-directional loading on shared anchors, this study developed a biaxial loading system with orthogonally arranged actuators. By independently controlling the load amplitudes and phase differences between two orthogonally arranged loading axes, cyclic loading with the resultant force varying around the mean direction within an angular range can be simulated, as illustrated in Figure 1. Specifically, sinusoidal cyclic loads are applied in both the X and Y axes, where the ratio of their amplitudes determines the mean direction of the resultant force. The angular range variation of the resultant force is controlled by adjusting the phase difference (φ) between the cyclic loads in the X and Y axes. In the current study, the load amplitudes in the X and Y axes were set equal, thus fixing the mean direction of the resultant force at 45º.

The multi-directional loading system and monitoring devices developed for the tests in sand and clay are shown in Figure 2 and Figure 3, respectively, while the shared pile anchor models used in experiments are shown in Figure 2(c) and Figure 3(b). The loading system mainly includes a strongbox, orthogonal dual-gantry reaction frames, actuators, a pulley system, a control cabinet, a control computer, and a data acquisition system. The sand strongbox and clay strongbox have internal dimensions of 3 m×3 m×2 m and 1.2 m×1.2 m×1.5 m (length × width × height). The orthogonal dual-gantry reaction frames can move along both X and Y directions through low-friction sliding rails. X and Y axes provide the loads, while the Z axis is used for jacking installation of pile anchors. All actuators are capable of performing both static and dynamic loading under either force-control or displacement-control conditions. Each actuator is equipped with a high-precision load cell at its end and has a built-in displacement encoder. The pulley system consists of upper pulleys adapted to the actuator height and lower pulleys that alter the inclined loading angle. All experimental data is acquired by the data acquisition system.

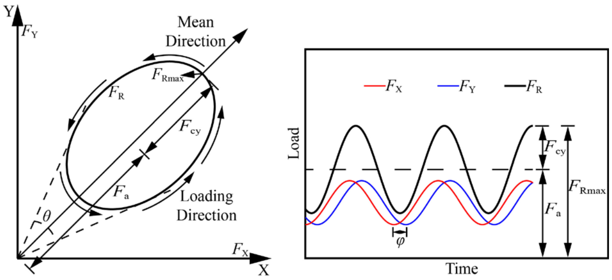

Figure 1 Cyclic loading with loading direction varies about the mean direction within an angular range

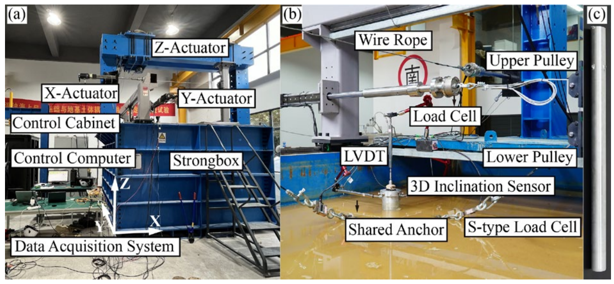

Figure 2 Testing set-up in sand: (a) the side view; (b) the top view; (c) the model pile anchor

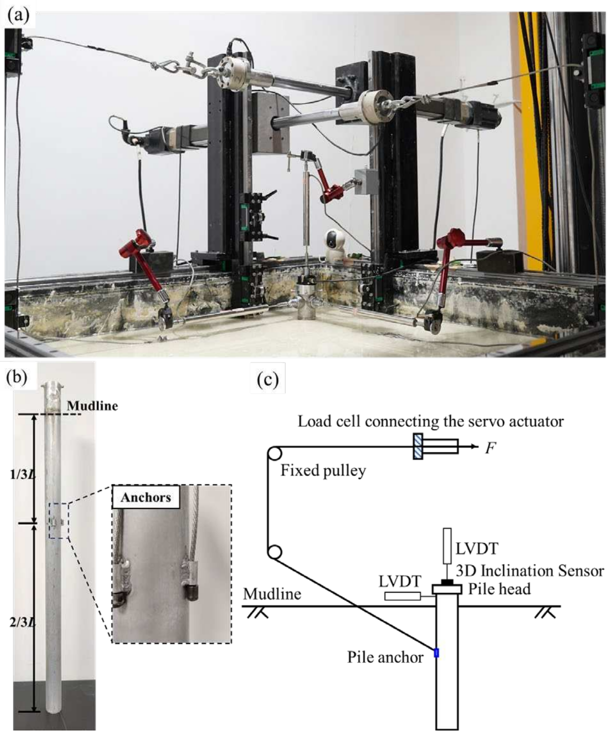

Figure 3 Testing set-up in clay: (a) the side view; (b) the model pile anchor (Note: L is the penetration depth); (c)

the simplified sketch for cross-section in the orthogonal direction

The X-axis and Y-axis horizontal actuators apply loads to the shared anchor through wire ropes. When the wire ropes change direction via pulleys, friction occurs, resulting in the actual load transmitted to the shared anchor being less than the load applied by the actuators. To address this issue, the actuator is controlled by the load cell located at the actuator end, while the load actually transmitted to the pile anchor is monitored by a S-type load cell connected at the wire rope termination.

The shared anchor exhibits 6-degree-of-freedom motion under orthogonal bidirectional loading. Three LVDTs with ball connections at both ends are employed for real time measurement of pile head displacements in X, Y and Z directions, as shown in Figure 2(b), Figure 3(a) and (c). The X-axis and Y-axis LVDTs are horizontally positioned above the mudline, while the Z-axis LVDT is vertically placed at the exact center of the pile head. Additionally, a 3D inclination sensor is employed to measure the anchor's inclination angles in X, Y and Z directions. The 3D inclination sensor has a measurement range of 0-360° with 0.01° resolution. It is mounted at the center of the anchor's top cover, which is fixed to the pile head with bolts.

2.2 Soil sample

2.2.1 Saturated sand sample

The tests utilized a natural fine river sand, and its physical parameters and gradation curve are presented in Table 1 and Figure 4. The sand mainly consists of quartz and feldspar, with particle shapes predominantly rounded to subrounded. The particle size ranges from 0-2 mm, with the majority falling between 0.075-2 mm.

The strongbox has a plan area of 9 m^2. Due to the large amount of sand required, the soil sample was prepared using a layered compaction method. The mass and water content of each sand bag (typically weighs about 1 tonne) was first measured. The target height of the compacted soil sample was then calculated based on the target relative density (65% for the current tests) and max and min void ratios determined in the laboratory. The final soil sample has a total height of 1.7 m. After sample preparation, saturation was achieved through water inlet pipes located at the bottom of the strongbox. During the tests, a constant free water head (5 cm) is maintained above the mudline. The effective unit weight of sand was measured to be 9.89 kN/m^3.

Six cone penetration tests (CPT) were conducted using a 5 cm^2 cone with a tip angle of 60°. The results are shown in Figure 5. The measured cone tip resistance profiles demonstrate excellent uniformity.

Table 1 Properties of the river sand adopted for model testing

Description	Values
Specific gravity: G_s	2.67
d_{50}: mm	0.23
Maximum void ratio: e_{max}	0.880
Minimum void ratio: e_{min}	0.534
Coefficient of nonuniformity: C_u	2.70
Coefficient of curvature: C_c	0.97
Peak internal friction angle: φ'_{peak}, °	36.9*

*Measured by isotopically consolidated drained triaxial compression test with an effective consolidation stress of 100 kPa on specimen of the same density as the soil bed for model testing.

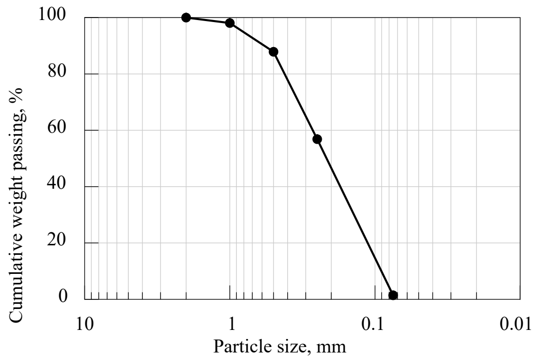

Figure 4 Grain size distribution curve of the river sand adopted for the tests

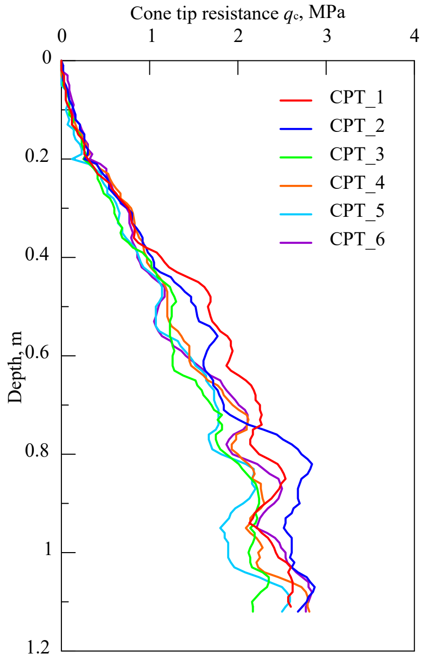

Figure 5 Cone tip resistance profiles of the sand sample

2.2.2 Clay sample

A clay sample was prepared by Malaysian kaolin with 1.3 m in height. The clay has a d_{60} of 0.006 mm and a plasticity index of 24.5% (the plastic and liquid limit are 37.5% and 62.0%, respectively).

Kaolin powder and water were mixed to produce a slurry with a water content of 130%. The slurry was then placed in the container and consolidated in stages under hydraulic pressure up to 75 kPa. Consolidation was deemed complete when no noticeable settlement was detected by the LVDT. To ensure adequate drainage during the consolidation stage, a 100 mm gravel layer was placed at the base of the container. Additionally, the drainage outlets at the bottom were left open. The top plate used for applying consolidation stress was perforated with 10 mm holes and wrapped in geotextile to facilitate drainage. After consolidation, the hydraulic pressure was released gradually, and the soil was allowed to swell before testing.

Figure 6 presents the undrained shear strength profile of the clay sample measured by CPT (5 cm^2 cone with a tip angle of 60^o) and T-bar penetrometer (25.2 mm in diameter and 126.1 mm in length). A N_{kt} factor of 14 and a $N_{t\text{-}bar}$ factor of 10.5 were used to derive the undrained shear from the CPT and T-bar tests, respectively. For interpretation of the T-bar test, the shallow correction proposed by White et al. (2010) was applied.

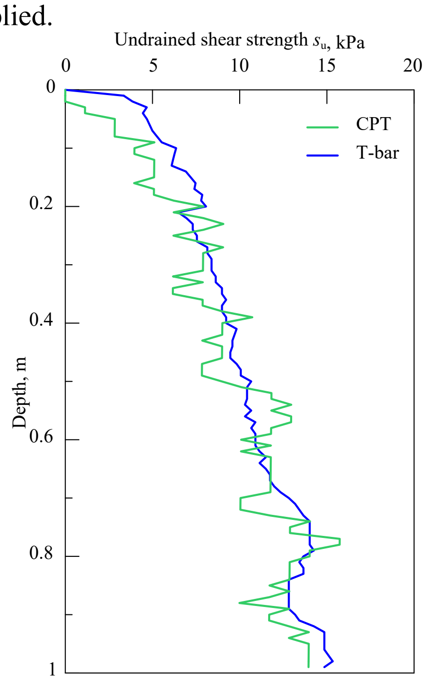

Figure 6 Undrained shear strength profiles of the clay sample

2.3 Model pile anchors

Scaled pile anchor models were adopted for tests in sand and clay, which were fabricated from aluminum alloy. The dimensions of the model piles and their prototypes are summarized in Table 2 and Table 3. The wall thicknesses of the pile anchors were determined by equivalence in bending stiffness, after considering the scaling relationship. To apply orthogonal bidirectional loading, two padeyes were equipped on the pile shaft, as shown by the photographs of the models in Figure 2(c) and Figure 3(b).

Table 2 Summary of the dimensions of the model pile anchor and the prototype for tests in sand

	D **(m)**	***WT*** **(m)**	***L*** **(m)**	***Z*****pad** **(m)**	***E*** **(GPa)**
Model	0.1	0.004	1.5	0.16	71.7
Prototype	2.5	0.030	37.5	4	210

Note: D is the external pile diameter; WT is the wall thickness; L is the penetration depth; Z_{pad} is depth of padeye below the mudline; E is the Young's modulus of the pile material.

Table 3 Summary of the dimensions of the model pile anchor and the prototype for tests in clay

	D **(m)**	***WT*** **(m)**	***L*** **(m)**	***Z*****pad** **(m)**	***E*** **(GPa)**
Model	0.055	0.002	1.0	0.33	71.7
Prototype	2.75	0.030	50	16.5	210

2.4 Load control

Based on the vector composition principle, the multi-directional loading on shared anchors can be simulated by two orthogonal loading components. As shown in Figure 7, the conversion between the resultant force (F_R) and the two inclined loading components (F_X, F_Y) is as follows:

$$F_R = F_X/(1+\tan^2(\beta)+2\tan(\beta)\sin^2(\alpha) \quad (1)$$

$$\beta = \arctan(F_Y/F_X) \quad (2)$$

$$\alpha_R = \arctan\left(\frac{\tan(\alpha)\cdot(1+\tan(\beta))}{(1+\tan^2(\beta))^{0.5}}\right) \quad (3)$$

where F_X and F_Y represent the inclined tension forces in X and Y directions respectively; α denotes the inclination angle between the wire rope and the horizontal plane; β denotes the angle between the vertical projection of F_R and the X-axis; α_R represents the inclination angle between the resultant force F_R and the horizontal plane.

In the current tests, the inclination angle between the wire rope and the horizontal plane is set to 30º for both X and Y loading axes based on experience. During testing, the inclination angle changes marginally due to anchor movement. However, no attempt was made to correct for this effect. The angle β depends on the relative load magnitudes of the two loading axes. In the current study, the mean value of β, denoted as β_m, is fixed at 45º in all tests.

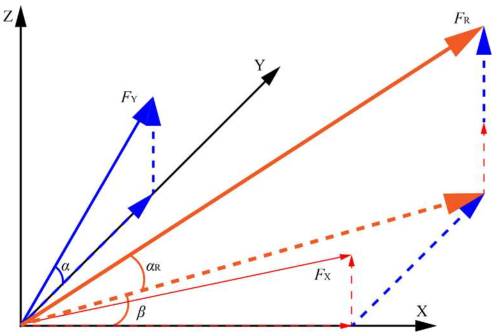

Figure 7 Spatial vector composition

2.5 Test programme

This study investigates the load-displacement characteristics of shared pile anchors under the loading condition with the resultant force direction varying within an angular range about the mean direction. The test programme consists of three tests each in sand and in clay, as summarized in Table 4 and Table 5 respectively. In all tests, the pile anchor was installed to the target penetration depth by jacking using the vertical actuator at 60 mm/min. Tests were then performed after sufficient waiting time (3 hours in sand and 8 hours in clay, respectively).

All cyclic tests employed a loading frequency of 0.1 Hz. Based on experience, the ratio of cyclic amplitude (F_{cy}) to mean value (F_a) of the resultant force was set at 0.6, as defined in Figure 1.

Table 4 summarizes the testing conditions in the sand sample. In tests M1, synchronized inclined loading was applied to the shared pile anchor in both X and Y axes until failure. The wire rope pulling rate was kept constant at 3 mm/min. Through test M1, the monotonic ultimate holding capacity of the model pile anchor was obtained, which was used to design the cyclic loading tests. Test C1 investigated the load-displacement response of the pile anchor under fixed-direction cyclic loading. In this test, the anchor received simultaneously cyclic loading from both X and Y directions with no phase difference between the two loading axes. In Test C2, the cyclic amplitude and cyclic number were kept identical to C1. The mean direction of the resultant force remained at 45º. However, due to a 39º phase difference set to the two axes, the resulting load path in the X-Y plane formed an ellipse, and the angle enclosed by the ellipse θ, as illustrated by Figure 1, was 18º.

Testing details in the clay sample are presented in Table 5. The wire rope pulling rate in Test M2 was kept constant at 48 mm/min to achieve the undrained conditions. Test C3 and Test C4 each consisted of four loading episodes (F_{Rmax}=20%F_u, 40%F_u, 60%F_u, 80%F_u), with 200 cycles applied in each episode. Test C3 was loaded by both axes with no phase difference in-between, resulting in a fixed direction loading condition. While in Test C4, a 60° phase difference is set to the X and Y loading axes. This results in an angular range of 45º.

Table 4 The testing programme in sand

Test ID	F_{Rmax}	β_m	φ	θ	F_{cy}/F_a	Cycle
M1	-	45º	-	-	-	-
C1	60%F_u	45º	-	-	0.6	2000
C2	60%F_u	45º	24º	18º	0.6	2000

Note: F_u represents the ultimate holding capacity of the shared pile anchor, determined as 6.67 kN based on test M1 in sand. φ and θ are defined in Figure 1.

Table 5 The testing programme in clay

Test ID	F_{Rmax}	β_m	φ	θ	F_{cy}/F_a	Cycle
M2	-	45º	-	-	-	-
C3	20~80% F_u	45º	-	-	0.6	800
C4	20~80% F_u	45º	60º	45º	0.6	800

Note: F_u represents the ultimate holding capacity of the shared pile anchor, determined as 2.0 kN based on test M2 in clay.

3 RESULTS IN SATURATED SAND

3.1 Results of monotonic loading test

The results of M1 are presented in Figure 8. The load history in both X and Y axis is presented in Figure 8(a). In the loading up to 0.5 kN, slight stiffness differences between the X and Y axis were observed. To ensure synchronous bidirectional loading, the system was switched from displacement control to force control to manually align the tension in the X and Y axis. The test was then returned to displacement control. The tensile loads in both directions remained highly consistent thereafter throughout the test, demonstrating both the effectiveness of the loading system and the uniformity of the soil sample. Figure 8(b) shows the resultant load-displacement curves. Figure 8(c) illustrates that the pile anchor experiences simultaneous large vertical and horizontal displacements, leading to a gradual extraction of the anchor foundation from the soil bed. Based on the resultant load-displacement curve, the ultimate holding capacity for pile anchors is determined to be 6.67 kN.

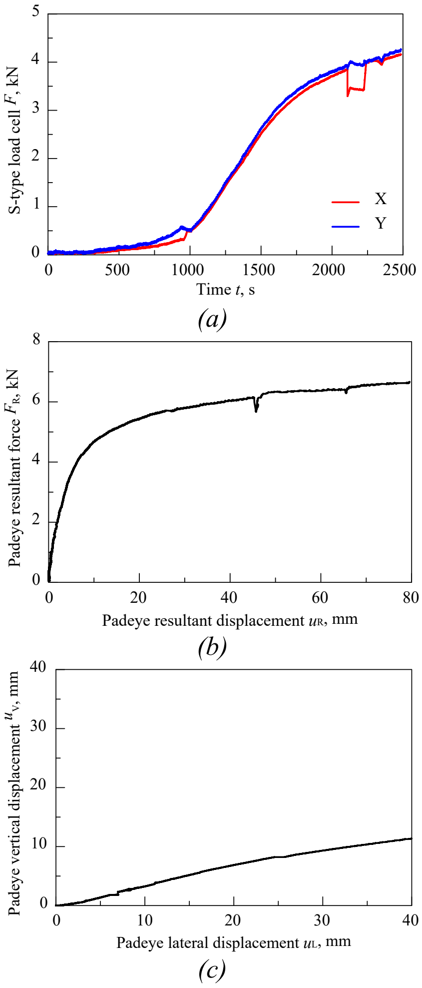

Figure 8 Results of monotonic test in sand: (a) load vs time at padeye; (b) resultant load vs displacement at padeye; (c) displacement trajectory at padeye

3.2 Results of cyclic loading tests

The results of C1 and C2 are presented in Figure 9. Figure 9(a) shows the cyclic loading path applied by the X and Y axis wire ropes in Test C2. The peak resultant force (F_{Rmax}) reached 60%F_u and the resultant loading direction varied within an 18º range around the mean direction of 45º for 2000 cycles. Figure 9(b) demonstrates that the cumulative horizontal displacement of the pile anchor is basically aligned with the mean direction of the resultant load in both cyclic tests. Figure 9(c) shows that the development trajectories of vertical and horizontal displacements of the pile anchors are essentially consistent between the two cyclic loading tests despite large differences in the magnitude. Figure 9(d) compares the progression of cumulative resultant displacement of the pile anchors with number of cycles between the two cyclic tests. During approximately the first 60 loading cycles, the results of the two tests are almost identical. However, at greater number of cycles, the test with direction varying within an 18º exhibits significantly accelerated rate of displacement accumulation.

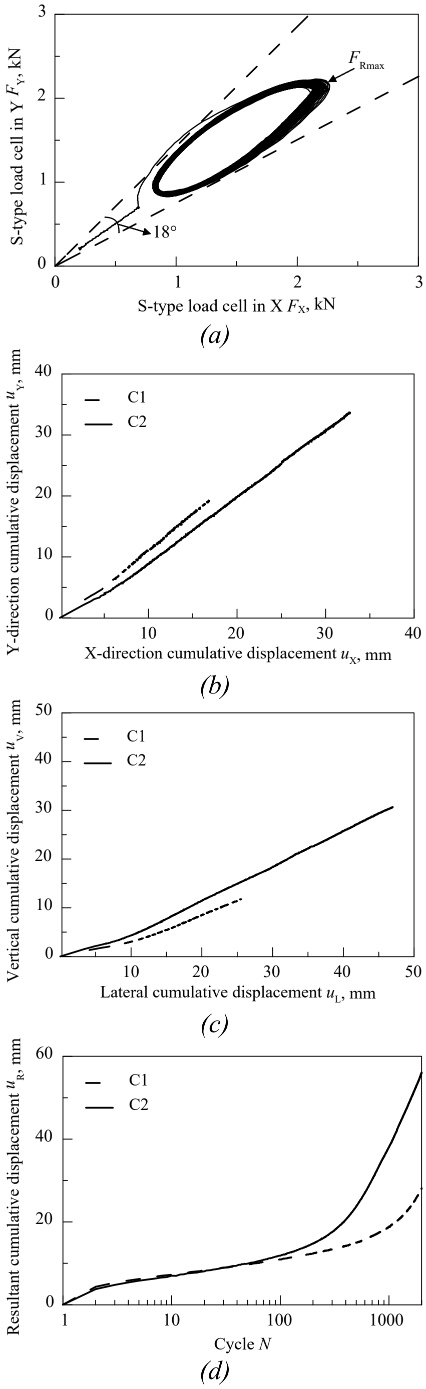

Figure 9 Results of cyclic tests in sand: (a) cyclic loading path of C2; (b) pile cumulative displacement in the horizontal plane; (c) pile cumulative displacement in space; (d) resultant cumulative displacement vs cycle number

4 RESULTS IN CLAY

Figure 10 (a) presents the resultant load-displacement curve of the monotonic loading test M2 in clay. The ultimate holding capacity of pile anchor was determined to be 2.0 kN beyond additional displacement produced only minimal increase in load. At the beginning, the displacement of pile head remained almost zero despite the increasing load. This is attributed to the high initial stiffness of the soil, large penetration length of the anchor and a padeye at 1/3 of the embedment, resulting in a flexible pile response. As the applied load increases, the pile behavior transits gradually from flexible to rigid response, which is caused by degradation of the soil stiffness with mobilization level.

Based on the ultimate holding capacity obtained from Test M2, four episodes (F_{Rmax}=0.4 kN, 0.8 kN, 1.2 kN, 1.6 kN, corresponding to 20%, 40%, 60% and 80% F_u respectively) were applied sequentially in both Tests C3 and C4. Test C3 maintained a constant loading direction, whereas in Test C4, the resultant loading direction varied within a 45° range around the mean direction of 45°, as illustrated by the loading path presented in Figure 10 (b). As presented in Figure 10 (d), when the peak resultant force is 20%F_u, the multi-directional loading effect can be practically ignored as the results from the two tests overlap on each other. However, at greater load levels, multi-directional loading accelerates the accumulation of displacement, and the effect intensifies with the load level.

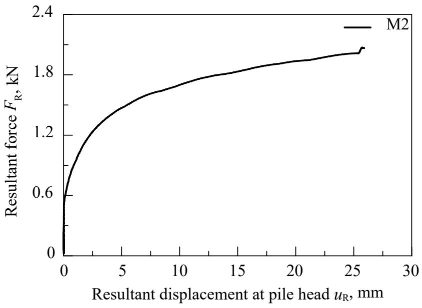

(a)

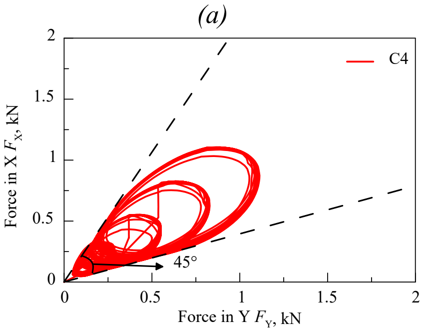

(b)

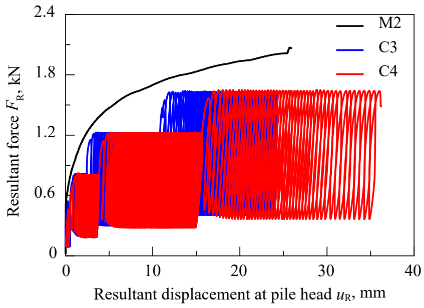

(c)

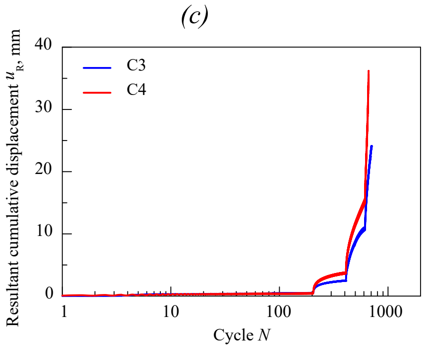

(d)

Figure 10 Tests results in clay: (a) pile deformation behavior; (b) cyclic loading path of C4; (c) resultant load vs displacement at pile head; (d) resultant cumulative displacement vs cycle number

5 CONCLUSIONS

Shared anchoring emerges as a promising technology for cutting down the cost of float offshore wind. In this study, a series of model tests in both saturated sand and clay is performed to investigate the failure mechanism and load-displacement behaviours of shared pile anchor under multi-directional loading conditions caused by phase differences between multiple mooring lines connected to the same anchor. Based on the test results, the following conclusions are drawn:

(1) For pile anchors in saturated sand and clay, the failure mechanism under multi-directional cyclic loading is similar to that under fixed-direction cyclic loading, featuring both vertical and horizontal cumulative displacements that increase gradually with number of loading cycles. The direction of the cumulative horizontal displacement is aligned with the mean direction of the resultant load on the anchor.

(2) In both sand and clay, the multi-directional loading is shown to accelerate the development of permanent displacement of the anchor under cyclic loading. This effect intensifies with the load level.

The results reported in this study highlights that in design of shared anchors, due consideration must be given to the detrimental effect caused by variation of the resultant cyclic loading direction experienced by the shared anchors.

ACKNOWLEDGEMENTS

The authors wish to gratefully acknowledge the financial support by the National Natural Science Foundation of China under Grant no. 52471273.

REFERENCES

Barron, J. R., Land, E., Rouainia, M., Charlton, T. S., Hu, Z., Ng, C., & Gibson, F. (2025). The performance of shared suction caisson anchors in sand for FOWT with taut mooring. *5th International Symposium on Frontiers in Offshore Geotechnics*, Nantes, France. https://doi.org/10.53243/ISFOG2025-549.

Chung, J. (2012). *Physical Modeling of Suction Caissons Loaded in Two Orthogonal Directions for Efficient Mooring of Offshore Wind Platforms*. Master thesis, The University of Maine.

Chalhoub, R., Jenck, O., Kochnev, A., Liaudat, J., Dano, C., Abadie, C. N., Szymkiewicz, F., Al Katabi, M. K., & H., Z. (2025). Floating wind turbine anchor piles under lateral multi-directional cyclic loading: experimental investigation. *5th International Symposium on Frontiers in Offshore Geotechnics*, Nantes, France. https://doi.org/10.53243/ISFOG2025-209.

Diaz, B. D., Rasulo, M., Aubeny, C. P., Fontana, C. M., Arwade, S. R., DeGroot, D. J., & Landon, M. (2016). Multiline anchors for floating offshore wind towers. *OCEANS 2016 MTS/IEEE Monterey*. https://doi.org/10.1109/OCEANS.2016.7761374.

Dias, X., Cerfontaine, B., & Wen, K. (2025). Finite element analysis of a shared pile anchor in sand under inclined multi-directional cyclic loading. *5th International Symposium on Frontiers in Offshore Geotechnics*, Nantes, France. https://doi.org/10.53243/ISFOG2025-68.

Fontana, C. (2019). *A Multiline Anchor Concept for Floating Offshore Wind Turbines*. https://doi.org/10.7275/13483708.

Fontana, C., Hallowell, S., Arwade, S., DeGroot, D., Landon, M., Aubeny, C., & Myers, A. (2019). Spatial coherence of ocean waves in multiline anchor systems for floating offshore wind turbines. *Ocean Engineering*. 184(15): 59-73. https://doi.org/10.1016/j.oceaneng.2019.04.048.

Frossard, R., Bendzovski, R., & Tuveng, E. (2025). Hywind Tampen – A geotechnical- and structural design of shared suction anchors, from concept to installation. *5th International Symposium on Frontiers in Offshore Geotechnics*, Nantes, France. https://doi.org/10.53243/ISFOG2025-402.

GWEC. (2022). *Global offshore wind report 2022*. June 2022.

Herduin, M. (2019). *Multi-directional loading on shared anchors for offshore renewable energy: Definition and preliminary investigation into soil behaviour and anchor performance*. https://doi.org/10.26182/5d2fd93d88ce7.

Huang, M., & Aggidis, G. A. (2008). Developments, expectations of wave energy converters and mooring anchors in the UK. *Journal of Ocean University of China*, 7(1), 10-16. https://doi.org/10.1007/s11802-008-0010-8.

Huang, L., Coughlan, K., Martinez, A., Wilson, D., Aubeny, C., Arwade, S., DeGroot, D., & Beemer, R. (2025). Centrifuge modelling of shared ring anchors for floating wind turbines subjected to cyclic loading in clay. *5th International Symposium on Frontiers in Offshore Geotechnics*, Nantes, France. https://doi.org/10.53243/ISFOG2025-336.

Jenck, O., Obaei, A., Emeriault, F., & Dano, C. (2021). Effect of Horizontal Multi-directional Cyclic Loading on Piles in Sand: A Numerical Analysis. *Journal of Marine Science and Engineering*, 9(2): 235. https://doi.org/10.3390/jmse9020235.

Lee, J. & Aubeny, C. (2020). Multiline Ring Anchor system for floating offshore wind turbines. *Journal of Physics: Conference Series*, Amherst, MA USA. 1452, 012036. https://doi.org/10.1088/1742-6596/1452/1/012036.

Lovera, A., Coquio, T., & Peyrard, C. (2025). Analysis of loads applied on floating wind turbines shared anchors. *Ocean Engineering*, 324, 120627. https://doi.org/10.1016/j.oceaneng.2025.120627.

White, D. J., Gaudin, C., Boylan, N., & Zhou, H. 2010. Interpretation of T-bar penetrometer tests at shallow embedment and in very soft soils. *Canadian Geotechnical Journal*, 47(2), 218–229. https://doi.org/10.1139/t09-096.

Xu, H., Rui, S., Shen, K., Jiang, L., Zhang, H., & Teng, L. (2024). Shared mooring systems for offshore floating wind farms: A review. *Energy Reviews*, 3(1), 100063. https://doi.org/10.1016/j.enrev.2023.100063.

Yan, B., Zhu, W., Gao, B., Ye, G., Tian, Y., & Wang, Y. (2024). Bearing capacity analysis and mechanism study of shared caisson under multi-directional loading. *Ocean Engineering*, 301, 117530. https://doi.org/10.1016/j.oceaneng.2024.117530.

Zabatta, R., Abadie, C. N., Blanc, M., Lerat, S., Jagu, A., & T., C. (2025). Centrifuge modelling of intermediate piles subjected to multi-directional cyclic lateral loading. *5th International Symposium on Frontiers in Offshore Geotechnics*, Nantes, France. https://doi.org/10.53243/ISFOG2025-318.